Inorganic Chemistry

Article

pubs.acs.org/IC

Synthesis and Structural Characterization of $RE_7Zn_{21}Tt_2$ (RE = La–Nd; Tt = Ge, Sn, and Pb): New Structure Type Among the Polar Intermetallic Phases

Nian-Tzu Suen and Svilen Bobev*

Department of Chemistry and Biochemistry, University of Delaware, 304A Drake Hall, Newark, Delaware 19716

Supporting Information

ABSTRACT: Reported are 11 new ternary phases with the general formula $RE_7Zn_{21}Tt_2$ (RE = La–Nd; Tt = Ge, Sn, and Pb), synthesized from the respective elements by reactions at high temperature. Their structures, established on the basis of single-crystal and powder X-ray diffraction work, are shown to be a new structure type with the orthorhombic space group *Pbam* (No. 55, Pearson symbol *oP*60). This complex atomic arrangement features condensed polyhedra made up of Zn atoms, interspersed by Ge, Sn, or Pb atoms in trigonal-planar coordination. The structure bears resemblance with the La_3Al_{11} and the $LaRhSn_2$ structure types, which are compared and discussed. Temperature dependent dc magnetization measurements confirm RE^{3+} ground states for all rare-earth elements, and the expected local-moment magnetism due to the partial filling of their 4f states for RE^{3+} = Ce^{3+}, Pr^{3+}, and Nd^{3+}. Theoretical considerations of the electronic structure based on the tight-binding linear muffin-tin orbital (TB-LMTO-ASA) method are also presented: the calculations support the experimental observation of a small, but not negligible, homogeneity range in $RE_7Zn_{21+x}Tt_{2-x}$ ($x < 0.5$). The partial substitution of the tetrel atoms by the electron-poorer Zn appears to be an important attribute, leading to an optimal valence electron concentration and, thereby, to the overall electronic stability of the crystal structure of this family of polar intermetallics.

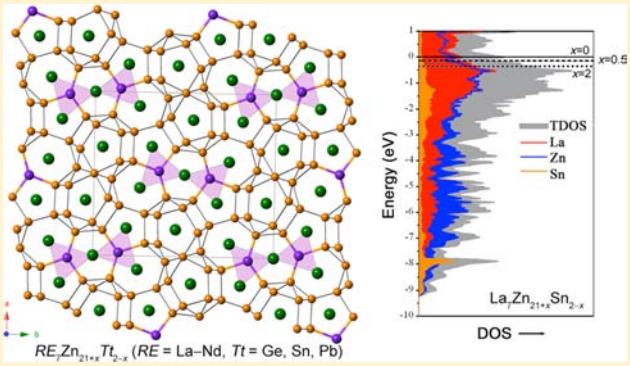

INTRODUCTION

Polar intermetallics provide excellent opportunities for the investigation of the relationships among crystal structures, electronic structures, and physical properties in extended solids.[1] Polar intermetallic compounds can be considered as the intermediate class between the valence compounds and the Zintl phases[2] on one hand, and the Hume–Rothery[3] or Laves phases[4] on the other. This view, which arguably is an oversimplification, draws on the fact that polar intermetallics attain electronic stability at certain valence electron concentration (VEC), as inferred from their density of states: Fermi level is typically located in a valley (pseudogap), although a separation between the valence band and conduction bands is lacking. Second, similar to the Zintl phases, the crystal structures of polar intermetallic compounds can be "separated" into (poly)anions and cations, although the latter usually participate in the covalent bonding, and, hence, do not donate all of their valence electrons. As a result, the bonding interactions in the polar intermetallic compounds are best viewed as multicenter bonds, in which the electrons are more delocalized compared to those in the Zintl phases, where the two-center two-electron model provides for a relatively good description.

As part of an ongoing program studying polar intermetallics (more specifically, rare-earth metal germanides), we have identified many new compounds in the ternary systems RE–Li–Ge,[5] RE–Mg–Ge,[6] RE–Al–Ge,[7] RE–In–Ge,[8] and RE–Sn–Ge.[9] Not long ago, we moved our exploratory studies one group farther to the left (into the d-block), and have already reported on the synthesis and the crystal structures of the new compounds RE_2CdGe_2 (RE = Y, Pr, Nd, Sm, Gd–Yb),[10] almost all of which are the first structurally characterized phases in the respective ternary RE–Cd–Ge systems. By comparison, the related RE–Zn–Ge systems appeared to have been studied in much greater detail with the following families of ternary phases being already known: REZnGe (RE = La–Tm),[11] $RE_2Zn_6Ge_3$ (RE = La–Sm),[12] $RE_4Zn_5Ge_6$ (RE = Gd–Lu),[13] and $RE_2Zn_3Ge_6$ (RE = La–Nd).[14] Therefore, we were initially reluctant to undertake work involving these elements; however, the discovery of the new stannides and plumbides RE_2Zn_5Tt (RE = La–Nd; Tt = Sn and Pb)[15] changed our intentions. In this Article, we present the fruition of our exploratory work in the zinc-rich sections of the RE–Zn–Ge phase diagrams. Subsequently, we extended the studies in the RE–Zn–Sn and RE–Zn–Pb phase diagrams, and herein, we detail the synthesis and the structural characterization of almost a dozen new ternaries with the general formula $RE_7Zn_{21+x}Tt_{2-x}$ ($x < 0.5$; RE

Received: July 31, 2013
Published: October 16, 2013

   dx.doi.org/10.1021/ic4019844 | *Inorg. Chem.* 2013, 52, 12731–12740

Table 1. Crystallographic Data and Refinement Parameters of $Ce_7Zn_{21}Tt_2$ (Tt = Ge, Sn, and Pb)

	$Ce_7Zn_{21.3}Ge_{1.7}$[a]	$Ce_7Zn_{21.28}Sn_{1.72(1)}$	$Ce_7Zn_{21.34}Pb_{1.66(1)}$
fw, g mol^{-1}	2496.62	2576.06	2720.48
crystal system	orthorhombic	orthorhombic	orthorhombic
space group	*Pbam* (No. 55) Z = 2	*Pbam* (No. 55) Z = 2	*Pbam* (No. 55) Z = 2
λ, Å	0.710 73	0.710 73	0.710 73
T, K	200(2)	200(2)	200(2)
a, Å	15.4457(15)	15.6455(4)	15.6927(19)
b, Å	17.0904(16)	17.2713(13)	17.342(2)
c, Å	4.4723(4)	4.4982(14)	4.4985(5)
V, Å^3	1180.6(2)	1215.5(4)	1224.2(2)
ρ_{calcd}, g cm^{-3}	7.023	7.039	7.380
μ(Mo Kα), cm^{-1}	364.3	350.3	445.2
GOF on F^2	1.188	1.158	1.139
R1 [$I > 2\sigma(I)$][b]	0.0170	0.0204	0.0174
wR2 [$I > 2\sigma(I)$][b]	0.0368	0.0380	0.0293
R1 (all data)[b]	0.0187	0.0224	0.0199
wR2 (all data)[b]	0.0373	0.0388	0.0299

[a]Zn and Ge having close X-ray scattering factors were not refined as mixed-occupied; the formula corresponds to the averaged composition from elemental analysis. [b]$R1 = \sum||F_o| - |F_c||/\sum|F_o|$; $wR2 = [\sum[w(F_o^2 - F_c^2)^2]/\sum[w(F_o^2)^2]]^{1/2}$, and $w = 1/[\sigma^2F_o^2 + (A\cdot P)^2 + B\cdot P]$, $P = (F_o^2 + 2F_c^2)/3$; A and B are weight coefficients.

= La–Nd; Tt = tetrel = Ge, Sn, and Pb). For brevity and simplicity hereafter, the compounds from this new series are referred to as $RE_7Zn_{21}Tt_2$, in accordance with the limiting, disorder-free composition. Structural relationships with other structure types are discussed, as well as the results from the electronic structure calculations and the magnetic susceptibility measurements.

EXPERIMENTAL SECTION

Synthesis. The starting materials [rare-earth metals (ingots), Ge (powder), Sn (shot), Pb (ingot), and Zn (shot)] were stored and handled inside an argon-filled glovebox in order to prevent their deterioration from moisture and oxygen. The elements were used as received, and were sourced from Alfa-Aesar or Acros with stated purity greater than 99.99% (with the exception of the lanthanides, which were purchased from Alfa-Aesar or Ames Laboratory with stated purity of 99.9%).

The first compounds from the new series were identified from reactions aimed to synthesize RE_2Zn_5Ge, the yet unknown analogues of RE_2Zn_5Tt (RE = La–Nd; Tt = Sn and Pb).[15] After analyzing the powder/single-crystal X-ray data, it was discovered that, instead of RE_2Zn_5Ge, the reaction products were mixtures of $RE(Zn_{1-x}Ge_x)_2$ (α-$ThSi_2$ structure type), $RE_7Zn_{21}Ge_2$ (new structure), and RE–Zn binary phases such as RE_3Zn_{11},[16] $RE_{13}Zn_{58}$,[17] and RE_2Zn_{17}.[18] These reactions required melting together mixtures of the respective elements. To avoid problems with the relatively low boiling point of Zn (b.p. 1180 K),[19] the elemental mixtures were enclosed in Nb containers, which had been sealed in both ends with an arc-welder. Subsequently, the Nb containers had to be jacketed in evacuated fused silica tubes (ca. 10^{-5} Torr). The reactions were carried out at 1173 K (heating rate of 200 K/h) for 12 h, followed by cooling to 1073 K over a period of 20 h, after which they cooled to room temperature by taking them out of the furnace.

Notice that, at this stage, the exact chemical make up of $RE_7Zn_{21}Ge_2$ was not clearly established since refining the single-crystal X-ray data was not unambiguous due to the close X-ray scattering factors of Ge and Zn.[20] We confirmed that the newly synthesized compounds are true ternary phases (not just RE_7Zn_{23} binaries, stabilized perhaps by small Ge inclusions) by attempting to synthesize RE_7Zn_{23} and $RE_7Zn_{22.5}Ge_{0.5}$, both of which failed. The yield of the target phase improved for a reaction with nominal stoichiometry $RE_7Zn_{22}Ge_1$, and appeared to have been maximized near the composition $RE_7Zn_{21}Ge_2$. To derive the correct stoichiometry, we ultimately synthesized $RE_7Zn_{21}Sn_2$, the structure refinements for which confirmed our working hypothesis.

Using the "7:21:2" ratio (rare-earth metal:Zn:Ge/Sn/Pb), we were able to successfully extend the series toward the corresponding plumbides. Although in this, and in all other cases, the desired phases were the major products, minor impurity phases were still apparent from the powder X-ray diffraction patterns. Therefore, we employed the same two-step method, which in earlier studies had offered the highest purity samples of RE_2Zn_5Tt (RE = La–Nd; Tt = Sn and Pb).[15] In the first step, we "prereacted" mixtures of the elements (in powder form, ground inside the glovebox to a homogeneous mixture) at lower temperature, 773 K for 24 h. Following this initial treatment, the pellets were brought in the glovebox, reground, and pressed again, after which they were annealed at 1073 K for 4 days. The powder X-ray diffraction patterns revealed the title compounds as the major product, except for the reaction aimed at $La_7Zn_{21}Ge_2$. The synthesis of this compound was not achieved, and the product appeared to be a mixture of $La(Zn_{1-x}Ge_x)_2$ (α-$ThSi_2$ structure type)[21] and $LaZn_4$ (own structure type).[22] The $RE_7Zn_{21}Tt_2$ (RE = La–Nd; Tt = Sn and Pb) samples all have minor impurity phase, RE_2Zn_5Tt (Tt = Sn and Pb).[15] This result is not surprising since RE_2Zn_5Tt and $RE_7Zn_{21}Tt_2$ (RE = La–Nd; Tt = Sn and Pb) are very close in terms of their chemical compositions and structures.

Subsequent attempts to extend this series to the mid-late rare-earth metals (beyond Sm) were unsuccessful; the products were common binary phases such as $RE_{13}Zn_{58}$,[17] $REZn_3$,[23] and RE_2Zn_{17}[18] (quite possibly being solid solutions $RE_2(Zn_{1-x}Tt_x)_{17}$ as reported for $Nd_2Zn_{15}Ge_2$,[24] for instance).

X-ray Powder Diffraction. X-ray powder diffraction data were taken at room temperature on a Rigaku MiniFlex powder diffractometer with Cu Kα radiation. Data analysis was done using the JADE 6.5 software package. The powder X-ray diffraction patterns of $RE_7Zn_{21}Tt_2$ (RE = La–Nd; Tt = Ge, Sn, and Pb) can be readily indexed, and the peak positions/intensities matched the simulations (on the basis of the single-crystal X-ray work). The powder X-ray diffraction patterns also indicated that the title compounds are stable in air for at least one month.

Single Crystal X-ray Diffraction. Single-crystal X-ray diffraction data were collected on a Bruker SMART CCD-based diffractometer equipped with a monochromated Mo Kα sealed-tube source. Crystals were selected under an optical microscope, cut to desired dimensions (<ca. 100 μm), and mounted on glass fibers with Paratone-N oil. Preliminary rotation images were acquired to assess the crystal quality. After that, full spheres of data were collected in four batch runs with frame width of 0.4° for ω and θ. Data acquisition and integration were

dx.doi.org/10.1021/ic4019844 | Inorg. Chem. 2013, 52, 12731–12740

done using the programs SMART[25] and SAINTplus,[26] respectively. Semiempirical absorption correction was fixed by using SADABS.[27] The structures were solved by direct methods, which located the positions of all atoms, and refined with full-matrix least-squares on F^2, as implemented in SHELXTL.[28] Refined parameters included the scale factor, extinction coefficients, atomic positions with the corresponding anisotropic displacement parameters, and occupation factors (where applicable). The refinements were straightforward, and convergence was easily achieved in virtually all cases.

However, there were some indications of potential disorder on one of the framework sites, which were not apparent for $RE_7Zn_{21}Ge_2$, but became very clear for $RE_7Zn_{21}Pb_2$: the site on which the Pb-atom is placed had too much electron density associated with it, and became ca. 90% occupied when its site occupation factor (SOF) was freed. In the case of $RE_7Zn_{21}Sn_2$, freeing the SOF for the Sn site led to ca. 95% occupancy, while the SOF for Ge in $RE_7Zn_{21}Ge_2$ was almost unchanged from full. Since the refinements for the Sn- and Pb-compounds in particular benefit from the better "X-ray contrast" (the X-ray scattering factors of Ge and Zn are very similar to be refined simultaneously),[20] we interpreted these observations as if the Tt-atoms were randomly mixed with Zn (as opposed to just being vacant), giving rise to the small, but not negligible homogeneity range in $RE_7Zn_{21+x}Tt_{2-x}$ ($x < 0.5$). The Tt−Zn disorder is rooted in the electronic structure, as discussed in detail later in this Article.

The atomic positions were standardized to STRUCTURE TIDY coordinates in the final refinement step.[29] Relevant details of the crystallographic investigations for $Ce_7Zn_{21}Ge_2$, $Ce_7Zn_{21}Sn_2$, and $Ce_7Zn_{21}Pb_2$ are listed in Table 1. Final atomic coordinates and equivalent isotropic displacement parameters for the same three compounds are given in Table 2; selected interatomic distances are tabulated in Table 3 and in Table 4, respectively. Analogous information for the remaining compounds is summarized in Tables S1−S9 in Supporting Information. CIF data have also been deposited with Fachinformationszentrum Karlsruhe, 76344 Eggenstein-Leopold-shafen, Germany [fax: (49) 7247-808-666; e-mail: crysdata@fiz.karlsruhe.de] with depository numbers CSD-426526 for $Ce_7Zn_{21}Ge_2$, CSD-426527 for $Pr_7Zn_{21}Ge_2$, CSD-426528 for $Nd_7Zn_{21}Ge_2$, CSD-426529 for $La_7Zn_{21}Sn_2$, CSD-426530 for $Ce_7Zn_{21}Sn_2$, CSD-426531 for $Pr_7Zn_{21}Sn_2$, CSD-426532 for $Nd_7Zn_{21}Sn_2$, CSD-426534 for $La_7Zn_{21}Pb_2$, CSD-426533 for $Ce_7Zn_{21}Pb_2$, CSD-426536 for $Pr_7Zn_{21}Pb_2$, and CSD-426535 for $Nd_7Zn_{21}Pb_2$.

Elemental Analysis. Several crystals from each reaction were selected and mounted on conductive carbon tape. The compositions of these crystals were analyzed with a JEOL 7400F electron microscope equipped with an INCA-OXFORD energy-dispersive spectrometer (EDS). The beam current was 10 μA at 15 kV accelerating potential, and the counting time for each spot was 240 s. The compositions of these crystals agreed well with the compositions established from single-crystal X-ray diffraction data.

Magnetic Susceptibility Measurements. Field cooled (FC) direct current (dc) magnetic susceptibility measurements were carried out using a physical property measurement system (PPMS). The magnetization (M) measurements were performed in the interval from 5 to 300 K in an applied magnetic field (H) of 3 kOe. The $RE_7Zn_{21}Ge_2$ samples (polycrystalline form, ca. 150−200 mg) were loaded in gel caps and secured with cotton to prevent them from moving under the magnetic field. $RE_7Zn_{21}Sn_2$ and $RE_7Zn_{21}Pb_2$ were not phase pure and could not be measured. The raw magnetization data were corrected for the holder contribution and converted to molar susceptibility ($\chi_m = M/H$). The net effective moments and Weiss temperatures were calculated from linear fits of the inverse magnetic susceptibility versus temperature.

Electronic Structure Calculations. To interrogate the chemical bonding, the electronic band structure of $La_7Zn_{21}Sn_2$ was computed with the Stuttgart TB-LMTO 4.7 program.[30] The total and partial density of states (DOS) and crystal orbital Hamiltonian populations (COHP)[31] of selected atomic interactions are presented herein. The local density approximation (LDA) was used to treat exchange and correlations.[32] No empty spheres were needed to meet the minimum overlapping criteria. The symmetry of the potential was considered

Table 2. Atomic Coordinates and Equivalent Isotropic Displacement Oarameters (U_{eq}[a]) for $Ce_7Zn_{21}Tt_2$ (Tt = Ge, Sn, and Pb)

atom	Wyckoff site	x	y	z	U_{eq} (Å^2)
$Ce_7Zn_{21}Ge_2$					
Ce1	4*h*	0.165 63(2)	0.179 94(2)	$^1/_2$	0.0051(1)
Ce2	4*h*	0.418 83(2)	0.261 04(2)	$^1/_2$	0.0079(1)
Ce3	4*g*	0.165 14(2)	0.454 29(2)	0	0.0055(1)
Ce4	2*b*	0	0	$^1/_2$	0.0068(1)
*T*1[b]	4*g*	0.020 99(4)	0.141 29(4)	0	0.0054(1)
Zn2	4*h*	0.072 15(5)	0.359 47(4)	0	0.0097(1)
Zn3	4*h*	0.247 44(5)	0.352 67(4)	$^1/_2$	0.0099(1)
Zn4	4*h*	0.300 02(5)	0.492 79(4)	$^1/_2$	0.0094(1)
Zn5	4*g*	0.352 80(5)	0.081 00(4)	$^1/_2$	0.0099(1)
Zn6	4*g*	0.075 63(5)	0.283 95(4)	$^1/_2$	0.0078(1)
Zn7	4*g*	0.153 07(5)	0.051 75(4)	0	0.0073(1)
Zn8	4*g*	0.258 00(5)	0.280 79(4)	0	0.0066(1)
Zn9	4*g*	0.304 32(5)	0.140 96(4)	0	0.0079(1)
Zn10	4*g*	0.363 85(5)	0.400 91(4)	0	0.0091(1)
Zn11	4*g*	0.466 07(5)	0.098 15(4)	0	0.0100(2)
Zn12	2*d*	0	$^1/_2$	$^1/_2$	0.0109(2)
$Ce_7Zn_{21}Sn_2$					
Ce1	4*h*	0.169 42(2)	0.181 40(2)	$^1/_2$	0.0044(1)
Ce2	4*h*	0.416 55(3)	0.253 72(2)	$^1/_2$	0.0081(1)
Ce3	4*g*	0.163 87(2)	0.455 11(2)	0	0.0046(1)
Ce4	2*b*	0	0	$^1/_2$	0.0065(1)
*T*1[b]	4*g*	0.019 44(3)	0.142 18(3)	0	0.0054(2)
Zn2	4*h*	0.074 82(6)	0.360 42(5)	0	0.0100(2)
Zn3	4*h*	0.250 01(5)	0.353 48(5)	$^1/_2$	0.0092(2)
Zn4	4*h*	0.298 65(5)	0.493 53(5)	$^1/_2$	0.0092(2)
Zn5	4*g*	0.351 85(5)	0.078 84(5)	$^1/_2$	0.0093(2)
Zn6	4*g*	0.078 79(5)	0.287 94(5)	$^1/_2$	0.0071(2)
Zn7	4*g*	0.157 40(5)	0.050 95(5)	0	0.0073(2)
Zn8	4*g*	0.257 59(5)	0.281 19(5)	0	0.0068(2)
Zn9	4*g*	0.305 53(5)	0.141 30(5)	0	0.0074(2)
Zn10	4*g*	0.357 77(5)	0.401 36(5)	0	0.0094(2)
Zn11	4*g*	0.466 71(5)	0.097 55(5)	0	0.0094(2)
Zn12	2*d*	0	$^1/_2$	$^1/_2$	0.0107(3)
$Ce_7Zn_{21}Pb_2$					
Ce1	4*h*	0.169 90(2)	0.181 52(2)	$^1/_2$	0.0052(1)
Ce2	4*h*	0.415 56(2)	0.253 28(2)	$^1/_2$	0.0092(1)
Ce3	4*g*	0.162 53(2)	0.455 56(2)	0	0.0054(1)
Ce4	2*b*	0	0	$^1/_2$	0.0076(1)
*T*1[b]	4*g*	0.018 44(2)	0.141 82(2)	0	0.0066(1)
Zn2	4*h*	0.074 07(5)	0.360 48(5)	0	0.0110(2)
Zn3	4*h*	0.249 06(5)	0.353 46(5)	$^1/_2$	0.0099(2)
Zn4	4*h*	0.298 39(5)	0.493 32(5)	$^1/_2$	0.0099(2)
Zn5	4*g*	0.351 87(5)	0.079 18(5)	$^1/_2$	0.0100(2)
Zn6	4*g*	0.079 71(5)	0.288 57(5)	$^1/_2$	0.0092(2)
Zn7	4*g*	0.159 45(5)	0.050 97(4)	0	0.0086(2)
Zn8	4*g*	0.257 34(5)	0.281 24(5)	0	0.0073(2)
Zn9	4*g*	0.305 82(5)	0.141 83(5)	0	0.0078(2)
Zn10	4*g*	0.355 23(5)	0.402 03(5)	0	0.0115(2)
Zn11	4*g*	0.466 45(5)	0.098 39(5)	0	0.0100(2)
Zn12	2*d*	0	$^1/_2$	$^1/_2$	0.0111(3)

[a] U_{eq} is defined as one-third of the trace of the orthogonalized U_{ij} tensor. [b] *T*1 is refined as a statistical mixture of Ge/Sn/Pb and Zn; for $Ce_7Zn_{21.3}Ge_{1.7}$, Ge:Zn ratio was constrained to be 0.85:0.15; for $Ce_7Zn_{21.28}Sn_{1.72(1)}$, Sn:Zn = 0.858(6):0.141; for $Ce_7Zn_{21.34}Pb_{1.66(1)}$ Pb:Zn = 0.832(2):0.167, respectively.

dx.doi.org/10.1021/ic4019844 | Inorg. Chem. 2013, 52, 12731−12740

Table 3. Selected Tt−Zn and Zn−Zn Distances (Å) in the $Ce_7Zn_{21}Tt_2$ (Tt = Ge, Sn, and Pb) Structures[a]

$Ce_7Zn_{21}Ge_2$					
atom pair	distance	atom pair	distance	atom pair	distance
*T*1−Zn10	2.532(1)	Zn3−Zn8 (2×)	2.5566(5)	Zn6−Zn8	2.817(1)
*T*1−Zn7	2.550(1)	Zn3−Zn10 (2×)	2.9855(7)	Zn6−Zn11	2.631(1)
*T*1−Zn6	2.580(1)	Zn4−Zn5	2.801(1)	Zn7−Zn9	2.790(1)
Zn2−Zn3	2.710(1)	Zn4−Zn7 (2×)	2.5575(5)	Zn7−Zn10	2.591(1)
Zn2−Zn6 (2×)	2.5824(5)	Zn4−Zn10 (2×)	2.9048(7)	Zn8−Zn9	2.494(1)
Zn2−Zn11 (2×)	2.8653(7)	Zn5−Zn9 (2×)	2.5712(5)	Zn8−Zn10	2.625(1)
Zn2−Zn12	2.6477(8)	Zn5−Zn11 (2×)	2.8543(7)	Zn9−Zn11	2.603(1)
Zn3−Zn4	2.529(1)	Zn5−Zn12	2.6618(8)	Zn11−Zn12 (2×)	2.8441(5)
$Ce_7Zn_{21}Sn_2$					
atom pair	distance	atom pair	distance	atom pair	distance
*T*1−Zn10	2.639(1)	Zn3−Zn8 (2×)	2.5751(8)	Zn6−Zn8	2.800(1)
*T*1−Zn7	2.672(1)	Zn3−Zn10 (2×)	2.9300(9)	Zn6−Zn11	2.643(1)
*T*1−Zn6	2.683(1)	Zn4−Zn5	2.778(1)	Zn7−Zn9	2.794(1)
Zn2−Zn3	2.744(1)	Zn4−Zn7 (2×)	2.5524(8)	Zn7−Zn10	2.595(1)
Zn2−Zn6 (2×)	2.5748(8)	Zn4−Zn10 (2×)	2.9066(9)	Zn8−Zn9	2.530(1)
Zn2−Zn11 (2×)	2.9062(9)	Zn5−Zn9 (2×)	2.5976(8)	Zn8−Zn10	2.601(1)
Zn2−Zn12	2.6798(9)	Zn5−Zn11 (2×)	2.8969(9)	Zn9−Zn11	2.633(1)
Zn3−Zn4	2.536(1)	Zn5−Zn12	2.6883(9)	Zn11−Zn12 (2×)	2.8580(8)
$Ce_7Zn_{21}Pb_2$					
atom pair	distance	atom pair	distance	atom pair	distance
*T*1−Zn10	2.6717(9)	Zn3−Zn8 (2×)	2.5777(6)	Zn6−Zn8	2.791(1)
*T*1−Zn7	2.7165(9)	Zn3−Zn10 (2×)	2.9231(8)	Zn6−Zn11	2.646(1)
*T*1−Zn6	2.7206(9)	Zn4−Zn5	2.789(1)	Zn7−Zn9	2.785(1)
Zn2−Zn3	2.749(1)	Zn4−Zn7 (2×)	2.5488(6)	Zn7−Zn10	2.593(1)
Zn2−Zn6 (2×)	2.5733(6)	Zn4−Zn10 (2×)	2.8916(8)	Zn8−Zn9	2.535(1)
Zn2−Zn11 (2×)	2.9017(8)	Zn5−Zn9 (2×)	2.6003(6)	Zn8−Zn10	2.598(1)
Zn2−Zn12	2.6844(9)	Zn5−Zn11 (2×)	2.8989(8)	Zn9−Zn11	2.631(1)
Zn3−Zn4	2.546(1)	Zn5−Zn12	2.6999(9)	Zn11−Zn12 (2×)	2.8719(5)

[a] *T*1 denotes the site on which Ge/Sn/Pb are statistically mixed with Zn.

spherical inside each Wigner−Seitz (WS) sphere,[33] and a combined correction was used to take into account the overlapping part. The radii of WS spheres were determined by an automatic procedure and were as follows: La = 2.09−2.21 Å, Zn = 1.41−1.61 Å, and Sn = 1.63 Å. The basis sets included 6s, 6p, 5d, and 4f orbitals for La; 4s, 4p, and 3d orbitals for Zn; and 5s, 5p, and 5d orbitals for Sn. The La 6p, Zn 3d, and Sn 5d orbitals were treated by the Löwdin downfolding technique.[33] The *k*-space integrations were done using the tetrahedron method, and the self-consistent charge density was obtained with 160 irreducible *k*-points in the Brillouin zone.

RESULTS AND DISCUSSION

Structure. $RE_7Zn_{21}Tt_2$ (RE = La−Nd; Tt = Ge, Sn and Pb) crystallize in the orthorhombic space group *Pbam* (Pearson symbol *oP*60), with a new structure type: a search in the Pearson's Handbook and in the Inorganic Crystals Structure Database (ICSD) did not return any known intermetallic phase with the same Wyckoff sequence. We have chosen to discuss the single-crystal data of $Ce_7Zn_{21}Ge_2$, $Ce_7Zn_{21}Sn_2$, and $Ce_7Zn_{21}Pb_2$ in Tables 1 and 2 (as representatives of the whole family), and the crystallographic parameters for the remaining 8 structures are provided as Supporting Information.

A schematic representation of the structure is shown in Figure 1. The structure is drawn in a way emphasizing the framework of covalently bonded zinc-tetrel atoms, with the lanthanide cations residing in the channels within it. There are 16 crystallographic sites in the asymmetric unit (Table 2): 4 for rare-earth metals, 11 for the Zn atoms, and 1 for the Ge, Sn, or Pb atoms, all in special positions. The latter site, as detailed in the Experimental Section, is a subject of small occupational disorder. The polyanionic substructure can be considered as made up of two building units: the first one is the 17-vertex polyhedron formed by Zn atoms, centered by a rare-earth metal atom, and the second one is the tetrel atoms, which reside in the centers of trigonal prisms of rare-earth metal atoms. The Tt-atoms are not isolated, but connected to three close-by Zn atoms in a trigonal-planar fashion. Two Zn_{17}-polyhedra are fused together via face sharing (Figure 2a, the shared face is highlighted in pink), and the larger 34-atom clusters are connected to each other through four Zn−Zn bonds between adjacent vertices in the *ab*-plane. The polyhedral Zn-only slabs have thickness equal to the crystallographic *c*-axis, and are stacked in this direction above each other, giving the framework a distinctive "open look", mostly originating from the formed pentagonal channels. Including the trigonal-planar Tt-atoms and the corresponding Zn−Tt bonds allows us to assemble the whole polyanionic framework, which has a rather complex topology.

Although the whole Zn_{17}-cluster seen here does not have a precedent with the Zn-polyhedra in other zinc-rich intermetallics, some other fragments of the structure can be associated with the structures of known compounds such as RE_2Zn_5Tt ($LaRhSn_2$ structure type)[15] and RE_3Zn_{11} (La_3Al_{11} structure type).[34] As seen in Figure 2a, the upper part of the Zn_{17}-polyhedron is composed of a six-membered Zn_6 ring with a boat-shape conformation and a capping Zn atom: this subunit also exists in RE_2Zn_5Tt. In RE_3Zn_{11}, a similar building unit can

dx.doi.org/10.1021/ic4019844 | *Inorg. Chem.* 2013, 52, 12731−12740

Table 4. Ce−Tt, Ce−Zn, and the Shortest Ce−Ce Distances (Å) in the $Ce_7Zn_{21}Tt_2$ (Tt = Ge, Sn, and Pb) Structures[a]

$Ce_7Zn_{21}Ge_2$					
atom pair	distance	atom pair	distance	atom pair	distance
Ce1−*T*1 (2×)	3.2293(6)	Ce2−Zn5	3.2416(9)	Ce3−Zn8	3.2940(8)
Ce1−Zn2	3.3909(8)	Ce2−Zn6 (2×)	3.3849(6)	Ce3−Zn9	3.2249(8)
Ce1−Zn3	3.2110(8)	Ce2−Zn8 (2×)	3.3593(6)	Ce3−Zn10	3.2020(9)
Ce1−Zn4	3.2422(8)	Ce2−Zn9 (2×)	3.5129(6)	Ce3−Zn11	3.1862(8)
Ce1−Zn5	3.3492(9)	Ce2−Zn10 (2×)	3.3816(6)	Ce3−Zn11	3.2027(8)
Ce1−Zn6 (2×)	3.1769(6)	Ce2−Zn11 (2×)	3.6445(7)	Ce3−Zn12 (2×)	3.4809(3)
Ce1−Zn7 (2×)	3.1366(6)	Ce3−Zn2 (2×)	3.1128(6)	Ce4−*T*1 (4×)	3.3070(5)
Ce1−Zn8 (2×)	3.1632(6)	Ce3−Zn3 (2×)	3.1036(6)	Ce4−Zn4 (2×)	3.0912(8)
Ce1−Zn9 (2×)	3.1674(6)	Ce3−Zn4 (2×)	3.1263(6)	Ce4−Zn7 (4×)	3.3723(6)
Ce2−*T*1 (2×)	3.2057(5)	Ce3−Zn5 (2×)	3.1252(6)	Ce4−Zn10 (4×)	3.5058(6)
Ce2−Zn2	3.1384(8)	Ce3−Zn6	3.2227(8)	Ce1−Ce2	3.9432(6)
Ce2−Zn3	3.0758(8)	Ce3−Zn7	3.2648(8)	Ce1−Ce4	4.0003(4)
$Ce_7Zn_{21}Sn_2$					
atom pair	distance	atom pair	distance	atom pair	distance
Ce1−*T*1 (2×)	3.3201(7)	Ce2−Zn5	3.186(1)	Ce3−Zn8	3.3433(5)
Ce1−Zn2	3.4282(9)	Ce2−Zn6 (2×)	3.4669(8)	Ce3−Zn9	3.2512(9)
Ce1−Zn3	3.229(1)	Ce2−Zn8 (2×)	3.3866(8)	Ce3−Zn10	3.1725(9)
Ce1−Zn4	3.283(1)	Ce2−Zn9 (2×)	3.4417(8)	Ce3−Zn11	3.1978(9)
Ce1−Zn5	3.3591(8)	Ce2−Zn10 (2×)	3.5222(9)	Ce3−Zn11	3.2160(9)
Ce1−Zn6 (2×)	3.2333(8)	Ce2−Zn11 (2×)	3.5986(9)	Ce3−Zn12 (2×)	3.4976(5)
Ce1−Zn7 (2×)	3.1890(8)	Ce3−Zn2 (2×)	3.1104(8)	Ce4−*T*1 (4×)	3.3438(6)
Ce1−Zn8 (2×)	3.1515(8)	Ce3−Zn3 (2×)	3.1553(8)	Ce4−Zn4 (2×)	3.1523(8)
Ce1−Zn9 (2×)	3.1738(8)	Ce3−Zn4 (2×)	3.1535(8)	Ce4−Zn7 (4×)	3.4493(8)
Ce2−*T*1 (2×)	3.2989(7)	Ce3−Zn5 (2×)	3.1122(8)	Ce4−Zn10 (4×)	3.5934(8)
Ce2−Zn2	3.1651(9)	Ce3−Zn6	3.1794(9)	Ce1−Ce2	4.0632(7)
Ce2−Zn3	3.1238(9)	Ce3−Zn7	3.2494(9)	Ce1−Ce4	4.1039(6)
$Ce_7Zn_{21}Pb_2$					
atom pair	distance	atom pair	distance	atom pair	distance
Ce1−*T*1 (2×)	3.3440(4)	Ce2−Zn5	3.1803(9)	Ce3−Zn8	3.3693(4)
Ce1−Zn2	3.4993(4)	Ce2−Zn6 (2×)	3.4959(8)	Ce3−Zn9	3.2683(9)
Ce1−Zn3	3.230(1)	Ce2−Zn8 (2×)	3.3850(7)	Ce3−Zn10	3.163(1)
Ce1−Zn4	3.302(1)	Ce2−Zn9 (2×)	3.4293(7)	Ce3−Zn11	3.1988(9)
Ce1−Zn5	3.3621(4)	Ce2−Zn10 (2×)	3.5510(8)	Ce3−Zn11	3.2160(9)
Ce1−Zn6 (2×)	3.2418(7)	Ce2−Zn11 (2×)	3.5934(8)	Ce3−Zn12 (2×)	3.4868(4)
Ce1−Zn7 (2×)	3.1955(6)	Ce3−Zn2 (2×)	3.1153(6)	Ce4−*T*1 (4×)	3.3454(4)
Ce1−Zn8 (2×)	3.1517(6)	Ce3−Zn3 (2×)	3.1683(7)	Ce4−Zn4 (2×)	3.1659(9)
Ce1−Zn9 (2×)	3.1753(7)	Ce3−Zn4 (2×)	3.1676(7)	Ce4−Zn7 (4×)	3.4788(7)
Ce2−*T*1 (2×)	3.3129(4)	Ce3−Zn5 (2×)	3.1155(6)	Ce4−Zn10 (4×)	3.6204(7)
Ce2−Zn2	3.1748(9)	Ce3−Zn6	3.1742(9)	Ce1−Ce2	4.0510(8)
Ce2−Zn3	3.1377(9)	Ce3−Zn7	3.2469(9)	Ce1−Ce4	4.1253(5)

[a] *T*1 denotes the site on which Ge/Sn/Pb are statistically mixed with Zn.

be found as well, however, without the capping Zn atom; the Zn_6 rings therefore are flattened compared to those in the title compounds. As noted in earlier publications, Zn−Zn bonding is versatile, and understandably, the corresponding Zn−Zn distances are wide ranging: they measure from 2.494(1) to 2.9855(7) Å in $Ce_7Zn_{21}Ge_2$; from 2.530(1) Å to 2.9300(9) Å in $Ce_7Zn_{21}Sn_2$; and from 2.535(1) Å to 2.9231(8) Å in $Ce_7Zn_{21}Pb_2$, respectively. The full set of distances are tabulated in Table 3, from which one can immediately see that the Zn−Zn bonds can be grouped into two subcategories. For example, in the case of $Ce_7Zn_{21}Ge_2$, one type of Zn−Zn bonds is represented with the shorter set ranging from 2.494(1) to 2.6618(8) Å (Figure 2a, emphasized as orange cylinder), while the second type are much longer, ranging from 2.710(1) to 2.9855(7) Å (Figure 2a, drawn as gray cylinders). On the basis of the Pauling covalent radius of Zn (r_{Zn} = 1.22 Å)[35] and the Zn−Zn contacts in the element form (d_{Zn-Zn} = 2.66 Å), it becomes apparent that one can distinguish the shorter as two-center two-electron (covalent) bonds, and the longer as multicenter configurations (delocalized).[36] This is a hallmark of the Zn−Zn interactions, as noted already, and is discussed for numerous structures, such as $RE_2Zn_6Ge_3$,[12] RE_2Zn_5Tt (RE = La − Nd; Tt = Sn and Pb),[15] Ce_3Zn_{11},[34] and $NaZn_{13}$,[37] to name just a few.

In contrast with the Zn−Zn bonding, the Zn−Tt interactions within the trigonal planar units (Figure 2b; Figure S2 in Supporting Information) bear only the characteristic features of the covalent bonds. The Ge−Zn6, Ge−Zn7, and Ge−Zn10 distances in the $Ce_7Zn_{21}Ge_2$ structure measure 2.580(1), 2.550(1), and 2.532(1) Å, respectively. The corresponding values for the Sn−Zn6, Sn−Zn7, and Sn−Zn10 bonds are 2.683(1), 2.672(1), and 2.639(1) Å, respectively. For

dx.doi.org/10.1021/ic4019844 | Inorg. Chem. 2013, 52, 12731−12740

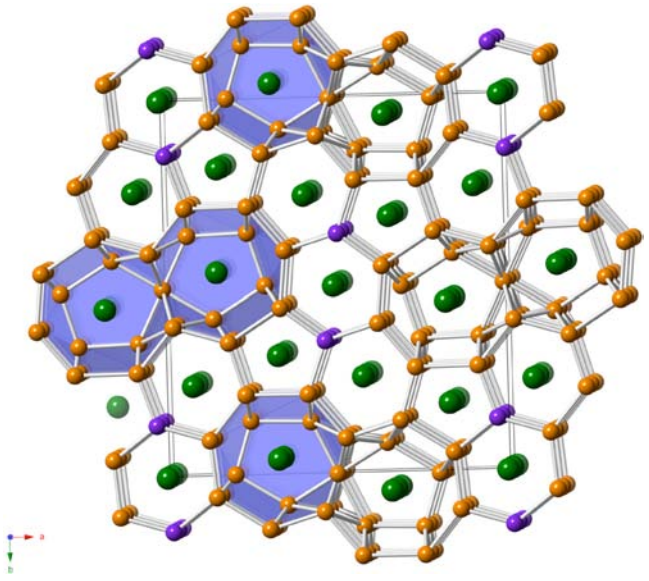

Figure 1. Combined polyhedral and ball-and-stick representation of the primitive orthorhombic structure of $Ce_7Zn_{21}Ge_2$, viewed down the [001] (approximate) direction. The Ce atoms are shown as green spheres, and the Zn atoms are drawn as orange spheres. The mixed occupied for Zn/Ge sites are emphasized in purple.

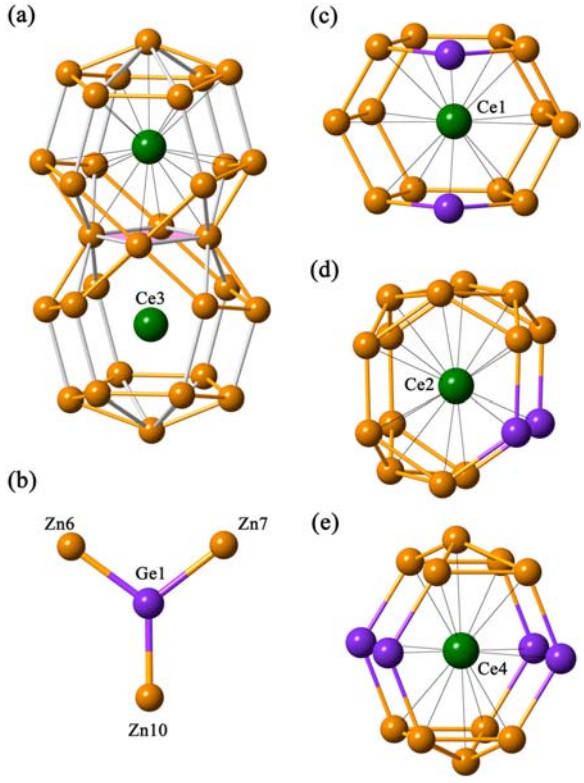

Figure 2. Close views of the main structural fragments of the structure of $Ce_7Zn_{21}Ge_2$: (a) 17-vertex Zn-cluster with Ce3 atoms encapsulated inside; (b) the trigonal-planar the Ge/Zn atom (site *T*1). The coordination polyhedra of Ce1 (c), Ce2 (d), and Ce4 (e). For the corresponding distances, the reader is referred to Tables 3 and 4.

$Ce_7Zn_{21}Pb_2$, the refinements yield 2.7206(9) Å for Pb−Zn6, 2.7165(9) Å for Pb−Zn7, and 2.6717(9) Å for Pb−Zn10. These values agree well with the sum of the corresponding Pauling radii ($r_{Ge} + r_{Zn}$ = 2.42 Å; $r_{Sn} + r_{Zn}$ = 2.61 Å; $r_{Pb} + r_{Zn}$ = 2.68 Å),[35] and match the distances reported in some ternary compounds such as $RE_4Zn_5Ge_6$ (RE = Gd−Tm),[13] RE_2Zn_5Tt (RE = La−Nd; Tt = Sn and Pb),[15] REZnSn,[38a] and CeZnPb,[38b] among others. The suggestion that the bonding interactions between Zn and Ge, Sn, or Pb are most likely covalent in nature is corroborated by the electronic structure calculations.

While the above considerations would be completely valid for the limiting, disorder-free $RE_7Zn_{21}Tt_2$, one must also consider the substitution of the tetrel element by Zn (up to 20%), when rationalizing the bonding. It is clear that, due to the electron configuration of the Zn atom, it might not favor the trigonal planar coordination environment of the tetrel atom, so the solubility range is expected to be limited. We did not do a case study probing the full range, but substantiate our point by the conclusions of You and Miller in their computational/experimental study of $Eu(Zn_{1-x}Ge_x)_2$ ($0 \le x \le 1$).[39] As shown on the latter examples, changes in the Ge/Zn ratio ultimately affect the coordination environment, where the end members $EuZn_2$ and $EuGe_2$ have the Zn and Ge in trigonal-pyramidal coordination, which changes to planar in the solid solution $Eu(Zn_{1-x}Ge_x)_2$, respectively.

The rare-earth metal atoms in the structure of $RE_7Zn_{21}Tt_2$ have diverse coordination environments, as shown in Figure 2. Among the four crystallographic sites, RE1 is 14-coordinated with 12 next-nearest Zn and 2 next-nearest Tt/Zn atoms. For RE2, the coordination environment resembles that of the Ba atom in $BaAl_4$, with one fewer atom (missing from the basal plane as shown in Figure S1 in Supporting Information). RE3 is enclosed within the Zn_{17} polyhedron, and the RE4 atom is sandwiched between two hexagonal rings with two additional Zn atoms. The Ce−Zn contacts [3.0758(8)−3.640(1) Å for $Ce_7Zn_{21}Ge_2$] are considerably longer than the sum of corresponding Pauling radii ($r_{Ce} + r_{Zn}$ = 2.86 Å),[35] which implies weak bonding interactions. Notice that the Ce−Zn and Ce−Tt distances correlate with the increased unit cell volume of the plumbide, over the stannide and germanide analogues. The RE−Zn and RE−Tt distances also "scale" with the decreasing size of the rare-earth element in the series La−Nd (i.e., the lanthanide contraction).

Considering that similar structural fragments can also be recognized in Ce_3Zn_{11},[34] and in Ce_2Zn_5Sn,[15] a brief comment on their structural relationship between the latter and $Ce_7Zn_{21}Tt_2$ (Tt = Ge, Sn, and Pb) is warranted here. As shown in Figure 3, $Ce_7Zn_{21}Tt_2$ can be viewed as the 1:2 intergrowth of Ce_3Zn_{11} and Ce_2Zn_5Sn, and the composition of title compounds can be understood according to the following equation:

$$Ce_7Zn_{21}Tt_2 = Ce_3Zn_{11} + 2 \times Ce_2Zn_5Tt$$

Electronic Structure. In order to understand the chemical bonding, electronic structure calculations of disorder-free $La_7Zn_{21}Sn_2$ and $La_7Zn_{21}Pb_2$ were performed using the TB-LMTO-ASA method.[30] Only the La-based compounds (as models for all other) were interrogated computationally, due to the known difficulties treating the partially filled 4f states for Ce, Pr, and Nd. The density of states (DOS) and crystal orbital Hamilton populations (COHP) curves for $La_7Zn_{21}Sn_2$ are presented and discussed next; the DOS for $La_7Zn_{21}Pb_2$, which closely resembles the one for the Sn-counterpart, is supplied as Supporting Information.

As seen in Figure 4a, there is no band gap between the valence and conduction bands, which indicates the metallic behavior of $La_7Zn_{21}Sn_2$. Assuming the rigid band model is valid,

dx.doi.org/10.1021/ic4019844 | *Inorg. Chem.* 2013, 52, 12731−12740

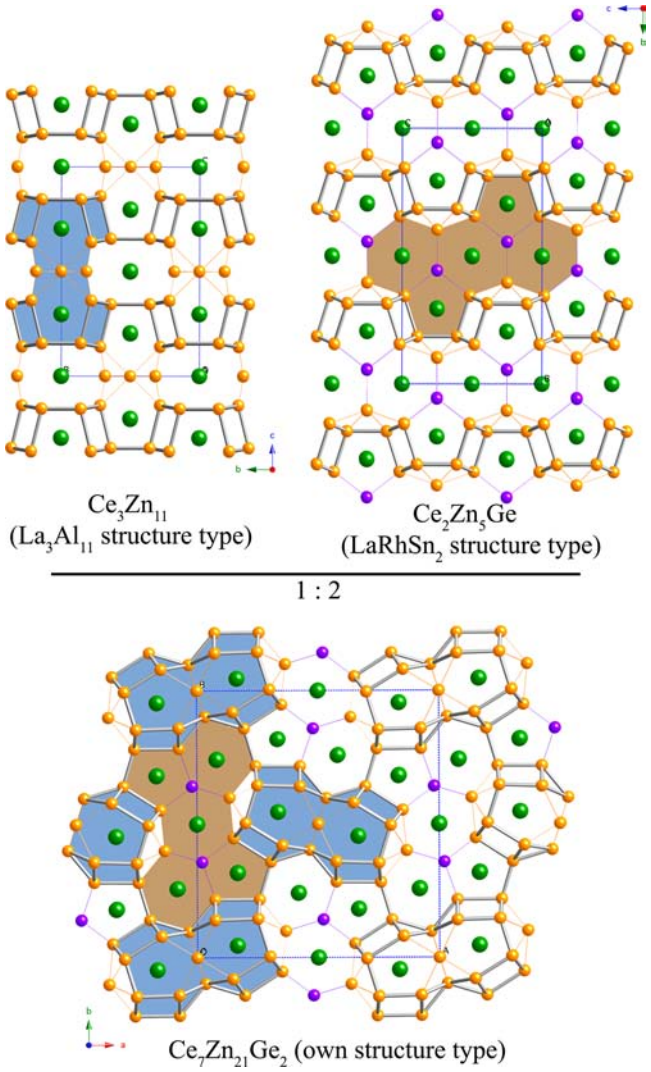

Figure 3. Schematic representation of the structural relationship between the new $Ce_7Zn_{21}Ge_2$, the known Ce_3Zn_{11} (La_3Al_{11} structure type), and a hypothetical Ce_2Zn_5Sn ($LaRhSn_2$ structure type) structures. $Ce_7Zn_{21}Ge_2$ can be viewed as an intergrowth of the latter two structures. To guide the eye in illustrating this idea, the cut-out from Ce_3Zn_{11} is highlighted in blue, and the fragment from Ce_2Zn_5Ge is shaded in brown.

we can integrate the number of valence electrons for several different compositions and place the Fermi level accordingly: these results are represented with three horizontal lines in the figure, corresponding to a count of 71 electrons/f.u. (solid line, idealized formula $La_7Zn_{21}Sn_2$), 70 electrons/f.u. (dashed line, formula representing 25% mixing of Tt/Zn and closer to the actual composition), and finally 67 electrons/f.u. (dotted line, La_7Zn_{23}). As mentioned already in the Experimental Section, all attempts to synthesize $RE_7Zn_{21+x}Tt_{2-x}$ with $x < 1$ failed, which is in perfect agreement with the calculations. The DOS curves for $La_7Zn_{21}Sn_2$ and La_7Zn_{23} show that the Fermi level falls in regions of relatively high DOS, which usually indicates the instability of the electronic structure. However, the Fermi level corresponding to the phase $La_7Zn_{21.5}Sn_{1.5}$ (70 valence electrons per formula) is a located in a region of relatively lower DOS. This feature of the electronic structure agrees very well with the experimental observation that introducing the tetrel atoms always partially replaces the electron poor Zn, thereby alleviating the electronic barrier to stabilize this phase.

The valence bands from La, Zn, and Sn exhibit significant overlap throughout the entire energy range, suggesting strong bonding interaction between these elements. These valence bands (Figure 4b–d) are mainly from the La 5d bands, Zn 4s, 4p bands and Sn 5s, 5p bands. Similar to La_2Zn_5Sn,[15] the 4s and 4p bands of Zn are highly dispersive due to the remarkably wide range of Zn–Zn distances. On the other hand, there is no significant overlap between the 5s and 5p bands of Sn, and this confirms the lack of s–p hybridization.[40,41a] The sharp spike around −9 eV in the DOS for $La_7Zn_{21}Pb_2$ (see Supporting Information) corresponds to the $6s^2$ lone pair of Pb, and is another testament to this conjecture.

On the basis of the COHP curves (Figure 4e,f), all the interactions at the Fermi level are in bonding states, and the Zn–Sn interactions are nearly optimized, suggesting strong covalency. Meanwhile, the highest −*i*COHP value of the Zn–Sn bonds (compared to all other pairs) also supports the fact that the tetrel atoms are critical, despite their low content (ca. 6% at.). Being a zinc-rich phase, it is not surprising that the Zn–Zn interactions in $La_7Zn_{21}Sn_2$ have the major contribution to the electronic structure in the proximity of the Fermi level. La–Zn and La–Sn interactions, albeit weak, also appear to contribute to a fair extent. This is a commonly seen feature in polar intermetallics,[1] allowing us to regard them as intermediate between the intermetallic and the Zintl phases. After all, in

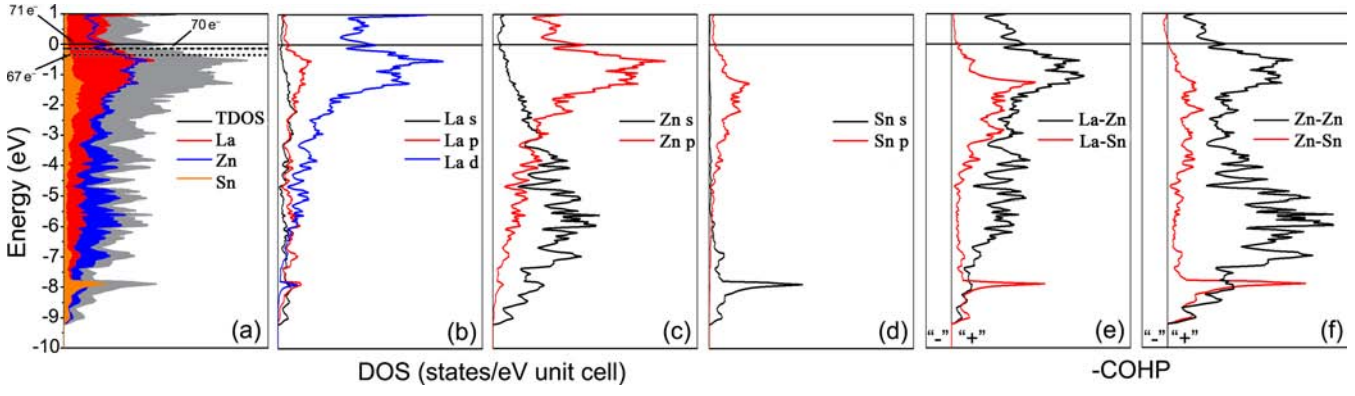

Figure 4. (a) Calculated total and partial DOS curves for $La_7Zn_{21}Sn_2$. The Fermi level is the energy reference at 0 eV. Partial DOS showing the s, p, and d bands contribution for La (b), Zn (c), and Sn (d). The COHP curves for La–Sn and La–Zn (e), and Zn–Zn and Zn–Sn (f) interactions. In the −COHP curves, the positive and negative signs represent bonding and antibonding states, respectively.

dx.doi.org/10.1021/ic4019844 | *Inorg. Chem.* 2013, 52, 12731–12740

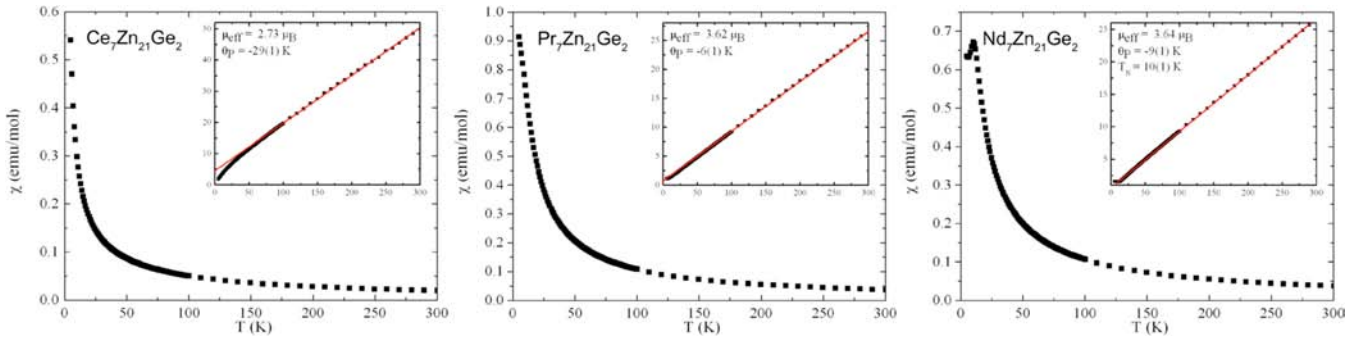

Figure 5. Field-cooled magnetic susceptibility vs temperature of $RE_7Zn_{21}Ge_2$ (RE = Ce–Nd). The insets show the temperature dependence of the inverse magnetic susceptibility. The red solid lines are the linear fits of the data, according to the Curie–Weiss law.

terms of chemical bonding, polar intermetallics are akin to both classes: above, we described the structure as La cations and Zn–Sn polyanionic framework, implicitly assuming predominantly covalent Zn–Sn interactions and mostly ionic La–Zn/La–Sn interactions. If we were to apply the Zintl concept[2] to $La_7Zn_{21}Sn_2$, in order to emphasize the Zn–Sn covalent bonding, its formula should be rationalized as $[La^{3+}]_7[Zn_{21}Sn_2]^{21-}$, meaning that the Zn and Sn will receive all three electrons from the La cations. However, the electronegativities of the elements are such (χ_P(La) = 1.0; χ_P(Zn) = 1.6; χ_P(Sn) = 1.8)[35] that the degree of polarization must be small. In other words, the notion that the La atoms are ionized and take the role of "spectators" or "electron donors" can be justified. This is also evident from the La–Zn/La–Sn COHPs, which, as shown in Figure 4, contribute significantly to the overall bonding. Therefore, with all the atoms being involved in multicenter interactions, it is not difficult to understand why the octet rule, i.e., the Zintl concept,[2] is not well-suited for rationalizing the structure of $La_7Zn_{21}Sn_2$. Arguably, if the atoms do not have closed-shell electronic configurations, the electron count will avoid description by the classic chemical ideas. Similar traits are commonly seen in the band structures of intermetallics containing late d-block metals, which are shown to receive electrons from less electronegative metals and behave as "pseudo-p-block elements".[41]

Magnetism. Only the germanide part of the $RE_7Zn_{21}Tt_2$ (RE = La–Nd; Tt = Ge, Sn, and Pb) series could be synthesized as single-phase material for measurements; therefore, only $Ce_7Zn_{21}Ge_2$, $Pr_7Zn_{21}Ge_2$, and $Nd_7Zn_{21}Ge_2$ were measured as part of this study. The temperature dependent dc magnetization measurements were performed on polycrystalline samples within the temperature range from 5 to 300 K in field cooling mode.

As seen from Figure 5, the magnetic responses for $Ce_7Zn_{21}Ge_2$, $Pr_7Zn_{21}Ge_2$, and $Nd_7Zn_{21}Ge_2$ in the high temperature regime follow the Curie–Weiss law $\chi(T) = C/(T - \theta_p)$,[42] where C is the Curie constant ($N_A\mu^2_{eff}/3k_B$) and θ_p is the Weiss temperature. The effective magnetic moments derived from the Curie constants are close to the theoretical values of free ion RE^{3+},[42] suggesting a local-moment 4f-magnetism due to Ce^{3+} ($4f^1$), Pr^{3+} ($4f^2$), and Nd^{3+} ($4f^3$).

In the low temperature regime, a cusp-like feature is apparent in the $\chi(T)$ for $Nd_7Zn_{21}Ge_2$, which suggests that the Nd^{3+} ions undergo magnetic ordering, likely entering into an antiferromagnetic ground state. The antiferromagnetic ordering is also confirmed from the negative Weiss temperature, the absolute value of which is in excellent agreement with the experimentally determined Néel temperature T_N = 10 K. Similar long-range magnetic ordering is not observed for $Ce_7Zn_{21}Ge_2$ and $Pr_7Zn_{21}Ge_2$, although the onset of spontaneous ordering (if there is any) might be seen if the measurements are taken at lower temperature.

A specific feature of the inverse susceptibility for $Ce_7Zn_{21}Ge_2$ must be pointed out: the fit of $1/\chi$ versus T deviates from linearity below ca. 40 K. This is a probable indicator of the presence of short-range ordering, similar to what was suggested for the related Ce_2Zn_5Sn compound.[15] The observed magnetic response can be understood by recalling the relatively long Ce–Ce distances (Table 4), which combined with the low J-values ($J = L + S = {}^5/_2$, i.e., the spin–orbit coupling) for the Ce^{3+} ion can account for the weak coupling between the magnetic moments. Nevertheless, the abnormally high paramagnetic Weiss temperature could mean that the magnetic coupling is more complex and could be due to competing effects in this sample. For example, we may speculate that the observed magnetism results from the competition between the local moment interactions mediated through the conduction electrons per the Ruderman–Kittel–Kasuya–Yosida (RKKY) mechanism,[42] the Kondo effect,[43] and even crystal field splitting of the ground state of the Ce^{3+} ion.[44] These phenomena are the hallmark of many Ce-containing intermetallics, such as $CeIn_3$,[45] $CeCo_2P_2$,[46] and $CeCoIn_5$,[47] among others, and call for further investigation of the low temperature physics of this new family.

■ CONCLUSION

The previous discovery of RE_2Zn_5Tt, followed by the herein discussed $RE_7Zn_{21}Tt_2$ (RE = La–Nd; Tt = Ge, Sn, and Pb) compounds, suggests that further exploratory work in these systems is worth pursuing as the available "phase-space" seems far from being exhausted. Owing to the "flexible" Zn–Zn bonding, the polyanionic framework of the newly discovered compounds displays adjustable character and ability to incorporate a variety of tetrel atoms, from Ge to Pb, despite the large difference in terms of their atomic sizes and orbital energies.

Our next target will be the systematic exploration of the RE–Zn–Si systems (RE = La–Nd), where, up until now, we have been able to obtain only $RE(Zn_{1-x}Si_x)_2$ (α-$ThSi_2$ structure type) solid solutions.[21] The issue to overcome here is the high melting point of silicon element and the low boiling point of zinc. More effort and other synthetic approaches will be required to resolve this synthetic challenge.

dx.doi.org/10.1021/ic4019844 | Inorg. Chem. 2013, 52, 12731–12740

■ ASSOCIATED CONTENT

Supporting Information

Combined X-ray crystallographic file in CIF format. Tables with interatomic distances in $RE_7Zn_{21}Tt_2$ (RE = La, Pr, and Nd; Tt = Ge, Sn, and Pb); a figure with a side-by-side comparison of structural fragments from the $Ce_7Zn_{21}Ge_2$ and $BaAl_4$ structure types; a plot of the Tt−Zn distances vs atomic sizes of tetrel elements in $Ce_7Zn_{21}Tt_2$ (Tt = Ge, Sn, and Pb) and Ce_2Zn_5Tt (Tt = Sn and Pb); a view of the $Ce_7Zn_{21}Ge_2$ structure with thermal ellipsoids, drawn at the 98% probability level; and DOS plot for $La_7Zn_{21}Pb_2$. This material is available free of charge via the Internet at http://pubs.acs.org.

■ AUTHOR INFORMATION

Corresponding Author

*E-mail: bobev@udel.edu. Phone: (302) 831-8720. Fax: (302) 831-6335.

Notes

The authors declare no competing financial interest.

■ ACKNOWLEDGMENTS

The authors gratefully acknowledge the financial support from the National Science Foundation, Grant DMR-0743916 (CAREER). We dedicate this paper to the memory of Professor John D. Corbett.

■ REFERENCES

(1) (a) Westbrook, J. H.; Fleischer, R. L. *Intermetallic Compounds: Principle and Practice*; Wiley: New York, 1995. (b) Schäfer, H. *Annu. Rev. Mater. Sci.* **1985**, *15*, 1. (c) Nesper, R. *Angew. Chem., Int. Ed. Engl.* **1991**, *30*, 789. (d) Guloy, A. M. Polar Intermetallics and Zintl Phases along the Zintl Border. *In Inorganic Chemistry in Focus III*; Wiley-VCH: Weinheim, Germany, 2006. (e) Corbett, J. D. *Inorg. Chem.* **2000**, *39*, 5178. (f) DiSalvo, F. J. *Pure Appl. Chem.* **2000**, *72*, 1799. (g) Corbett, J. D. *Inorg. Chem.* **2010**, *49*, 13.

(2) (a) Zintl, E. *Angew. Chem.* **1939**, *52*, 1. (b) Kauzlarich, S. M., Ed. *Chemistry, Structure and Bonding of Zintl Phases and Ions*; VCH Publishers: New York, 1996 and references therein.

(3) (a) Hume-Rothery, W.; Powell, H. M. *Z. Kristallogr.* **1935**, *91*, 23. (b) Hoistad, L. M.; Lee, S. *J. Am. Chem. Soc.* **1991**, *113*, 8216.

(4) Laves, F.; Witte, H. *Metallwirtsch., Metallwiss., Metalltech.* **1936**, *15*, 840.

(5) (a) Bobev, S.; You, T.-S.; Suen, N.-T.; Saha, S.; Greene, R.; Paglione, J. *Inorg. Chem.* **2012**, *51*, 620. (b) You, T.-S.; Bobev, S. *J. Solid State Chem.* **2010**, *183*, 2895. (c) Guo, S.-P.; You, T.-S.; Bobev, S. *Inorg. Chem.* **2012**, *51*, 3119. (d) Guo, S.-P.; You, T.-S.; Jung, Y.-H.; Bobev, S. *Inorg. Chem* **2012**, *51*, 6821.

(6) (a) Suen, N.-T.; Tobash, P. H.; Bobev, S. *J. Solid State Chem.* **2011**, *184*, 2941. (b) Tobash, P. H.; Bobev, S.; Thompson, J. D.; Sarrao, J. L. *Inorg. Chem.* **2009**, *48*, 6641. (c) Tobash, P. H.; Bobev, S. *J. Am. Chem. Soc.* **2006**, *128*, 3532.

(7) Zhang, J.; Bobev, S. *Inorg. Chem.* **2013**, *52*, 5307.

(8) (a) Tobash, P. H.; Lins, D.; Bobev, S.; Lima, A.; Hundley, M. F.; Thompson, J. D.; Sarrao, J. L. *Chem. Mater.* **2005**, *17*, 5567. (b) You, T.-S.; Tobash, P. H.; Bobev, S. *Inorg. Chem.* **2010**, *49*, 1773.

(9) Tobash, P. H.; Meyers, J. J.; Difilippo, G.; Bobev, S.; Ronning, F.; Thompson, J. D.; Sarrao, J. L. *Chem. Mater.* **2008**, *20*, 2151.

(10) Guo, S.-P.; Meyers, J. J.; Tobash, P. H.; Bobev, S. *J. Solid State Chem.* **2012**, *192*, 16.

(11) Pani, M.; Manfrinette, P.; Palenzona, A. *Intermetallics* **2009**, *17*, 146.

(12) Grytsiv, A. V.; Bauer, E.; Berger, S.; Hilscher, G.; Michor, H.; Paul, C.; Rogl, P.; Daoud Aladine, A.; Keller, L.; Roisnel, T.; Noel, H. *J. Phys.: Condens. Matter* **2003**, *15*, 3053.

(13) (a) Kranenberg, C.; Johrendt, D.; Mewis, A. *Z. Anorg. Allg. Chem.* **2001**, *627*, 539. (b) Fritsch, V.; Moreno, N. O.; Thompson, J. D.; Sarrao, J. L.; Bobev, S. *J. Magn. Magn. Mater.* **2006**, *299*, 87. (c) Reker, B.; Johrendt, D.; Pöttgen, R. *Intermetallics* **2013**, *38*, 36.

(14) Salvador, J. R.; Bilic, D.; Gour, J. R.; Mahanti, S. D.; Kanatzidis, M. G. *Inorg. Chem.* **2005**, *44*, 8670.

(15) Suen, N.-T.; Bobev, S. *Inorg. Chem.* **2013**, *52*, 9102.

(16) Chiotti, P.; Lott, B. G. *Acta Crystallogr.* **1966**, *20*, 733.

(17) Piao, S.; Gómez, C. P.; Lidin, S. *Z. Kristallogr.* **2006**, *221*, 391.

(18) Siegrist, T.; Le Page, Y. *J. Less-Common Met.* **1987**, *127*, 189.

(19) *CRC Handbook of Chemistry and Physics*, 83rd ed.; CRC Press LLC: Boca Raton, FL, 2002.

(20) Morre, F. H. *Acta Crystallogr.* **1963**, *16*, 1169.

(21) *Pearson's Handbook of Crystallographic Data for Intermetallic Phases*, 2nd ed.; Villars, P., Calvert, L. D., Eds.; American Society for Metals: Materials Park, OH, 1991.

(22) Oshchapovsky, I.; Paylyuk, V.; Dmytriv, G.; Griffin, A. *Acta Crystallogr., Sect. C* **2012**, *68*, 137.

(23) Bruzzone, G.; Fornasini, M. L.; Merlo, F. *J. Less-Common Met.* **1970**, *22*, 253.

(24) Demchenko, P.; Bodak, O. *Pol. J. Chem.* **2001**, *75*, 153.

(25) *SMART NT, version 5.63*; Bruker Analytical X-ray Systems, Inc.: Madison, WI, 2003.

(26) *SAINT NT, version 6.45*; Bruker Analytical X-ray Systems, Inc.: Madison, WI, 2003.

(27) *SADABS NT, version 2.10*; Bruker Analytical X-ray Systems, Inc.: Madison, WI, 2001.

(28) *SHELXTL, version 6.12*; Bruker Analytical X-ray Systems, Inc.: Madison, WI, 2001.

(29) Gelato, L. M.; Parthé, E. *J. Appl. Crystallogr.* **1987**, *20*, 139.

(30) Jepsen, O.; Burkhardt, A.; Andersen, O. K. *The TB-LMTO-ASA Program, version 4.7*; Max-Planck-Institute für Festkörperforschung: Stuttgart, Germany, 1999.

(31) Dronskowski, R.; Blöchl, P. *J. Phys. Chem.* **1993**, *97*, 8617.

(32) von Barth, U.; Hedin, L. *J. Phys. C: Solid State Phys.* **1972**, *5*, 1629.

(33) Andersen, O. K.; Jepsen, O.; Glötzel, D. *Highlights of Condensed Matter Theory*; Bassani, F., Fumi, F., Tosi, M., Eds.; North-Holland: New York, 1985.

(34) Malik, Z.; Sologub, O.; Giester, G.; Rogl, P. *J. Solid State Chem.* **2011**, *184*, 2840.

(35) Pauling, L. *The Nature of the Chemical Bond*; Cornell University Press: Ithaca, NY, 1960.

(36) (a) Zheng, C.; Hoffmann, R. *Z. Naturforsch.* **1986**, *41b*, 292. (b) Burdett, J. K.; Miller, G. J. *Chem. Mater.* **1990**, *2*, 12.

(37) (a) Zintl, E.; Haucke, W. *Z. Elektrrochem. Angew Phys. Chem.* **1938**, *44*, 104. (b) Gupta, S.; Corbett, J. D. *Inorg. Chem.* **2012**, *51*, 2247.

(38) (a) Manfrinetti, P.; Pani, M. *J. Alloys Compd.* **2005**, *393*, 180. (b) Hermes, W.; Rodewald, U. C.; Chevalier, B.; Matar, S. F.; Eyert, V.; Pöttgen, R. *Solid State Sci.* **2010**, *12*, 929.

(39) You, T.-S.; Lidin, S.; Gourdon, O.; Wu, Y.; Miller, G. J. *Inorg. Chem.* **2009**, *48*, 6380.

(40) The speculated lack of s−p hybridization is not due to symmetry considerations. Instead, the relatively high energy separation between the 5s and 5p states causes the ineffective overlap. This is particularly well manisfested by the "lone pair effect" in Pb, but also applicable to Sn and Ge. See, for example: (a) Kim, S.-J.; Kraus, F.; Fässler, T. F. *J. Am. Chem. Soc.* **2009**, *131*, 1469. (b) Takahashi, M. *Symmetry* **2010**, *2*, 1745.

(41) (a) Whangbo, M.-H.; Lee, C.; Köhler, J. *Angew. Chem., Int. Ed.* **2006**, *45*, 7465. (b) Köhler, J.; Whangbo, M.-H. *Chem. Mater.* **2008**, *20*, 2751. (c) Lee, C.; Whangbo, M.-H.; Köhler, J. *Z. Anorg. Allg. Chem.* **2010**, *636*, 36.

(42) (a) Smart, J. S. *Effective Field Theories of Magnetism*; Saunders, Philadelphia, PA, 1966. (b) Kittel, C. *Introduction to Solid State Physics*, 7th ed.; John Wiley and Sons: Hoboken, NJ, 1996.

(43) Kondo, J. *Prog. Theor. Phys.* **1964**, *32*, 37.

(44) Dunn, T. M.; McClure, D. S.; Pearson, R. G. *Some Aspects of Crystal Field Theory*; Harper & Row: New York, 1965.

(45) Buschow, K. H. J.; de Wijn, H. W.; van Diepen, A. M. *J. Chem. Phys.* **1969**, *50*, 137.
(46) Reehuis, M.; Jeitschko, W. *J. Phys. Chem. Solids* **1990**, *51*, 961.
(47) Petrovic, C.; Pagliuso, P. G.; Movshovich, R.; Sarrao, J. L.; Thompson, J. D.; Fisk, Z.; Monthoux, P. *J. Phys.: Condens. Matter* **2001**, *13*, L337.